arXiv:1302.1117v1 [nucl-ex] 5 Feb 2013

Heavy Nuclei Photofission at Intermediate Energies

A. Deppman,* E. Andrade-II,† V. Guimarães,‡ and G. S. Karapetyan§
Instituto de Física, Universidade de São Paulo, P. O. Box 66318, 05315-970 São Paulo, SP, Brazil

N. A. Demekhina¶
Yerevan Physics Institute, Alikhanyan Brothers 2, Yerevan 0036, Armenia
Joint Institute for Nuclear Research (JINR), Flerov Laboratory of Nuclear Reactions (LNR), Joliot-Curie 6, Dubna 141980, Moscow region Russia

In the present work the yields of fission fragments, from Bremsstrahlung induced fission of ^{232}Th, ^{238}U targets, were reproduced by CRISP model calculations, to which a multimodal fission option had been added. An extension of the calculation to the properties of the fission products is presented. Dividing the fissioning nuclei according to their fissionability, an approach which accounts for the contribution of symmetric and asymmetric fission is introduced. It allows to calculate the main parameters of the fission fragment charge distribution: the most probable charge for a given fission product mass chain and the width parameter. Furthermore, it reproduces the features of fragment mass distribution, and evaluates the fissility of fissioning nuclei in photon-induced fission. A comparison between the results of this calculation and experimental data is accomplished.

PACS numbers: 25.85.Jg

I. INTRODUCTION

Despite almost one hundred years of investigations about nuclear fission, this process still arises much interest. The disintegration of the nucleus into two fragments of similar masses is accompanied by a complete rearrangement of the nuclear structure. The dynamical process leading to fission determines the characteristics of the fragments in the final states.

Investigation of the photofission process in heavy nuclei purports an increasing interest, not solely for the investigation of fission itself, but furthermore to obtain information about the total photoabsorption. Photons provide a convenient tool to study the nuclear properties of a fissile system, since electromagnetic interaction is the subtlest and most adequate technique for exploring nuclear transformations at large deformations. In the case of photonuclear reactions, volume absorption dominates, and as a result, a photon effectively "heats" the nucleus. For this reason, the nucleus excitation in different energy ranges reflects the nature of the interaction with the incident photon. In reactions with heavy targets, where the fission probability is close to unit, this fact allows to obtain information about the photoabsorption cross-section.

The determination of the fission cross-section within different models, and the comparison with the experimental data as well, provides an opportunity to estimate the validity of the various photoabsorption mechanisms representation, as well as to investigate the characteristics of this process in the reactions by different probes. Such characteristics include the charge and the mass distribution of the fragments, the energy dependence of the fission cross-section, and the ratio of symmetric and asymmetric components of fission products, for instance. In the experiments with Bremsstrahlung, for the calculations of total photofission yields, the contributions of the different interaction modes are taken into account by summing over the entire spectrum of photons. The excited nuclei can decay by the well known "standard evaporation" and the conventional fission, allowing the study of prominent fission and evaporation mechanisms.

In the present work, CRISP model calculations of fragment distributions, produced in photofission of heavy nuclei (^{232}Th, ^{238}U) induced by Bremsstranhlung at end-point energies 50 and 3500 MeV are presented. Comparison with experimental data is determined, in order to get a complete description of multimodal fission for photon-induced reactions. The experiments considered were described in detail elsewhere [1, 2].

*Electronic address: deppman@if.usp.br
†Electronic address: esegundo@if.usp.br
‡Electronic address: valdirg@dfn.if.usp.br
§Electronic address: ayvgay@ysu.am
¶Electronic address: demekhina@nrmail.jinr.ru

II. THE CRISP CODE

CRISP is a Monte Carlo code for simulating nuclear reactions [3] that uses a two step process. First, an intranuclear cascade is simulated, following a time-ordered sequence of collisions in a many-body system [4, 5]. Besides, when the intranuclear cascade finishes, the evaporation of nucleons and alpha-particles starts to compete with fission [6].

In the simulation, the reactions can be initiated by intermediate and high energy protons [5] or photons [7–9]. It has been extended to energies up to 3.5 GeV [10], and it was shown that the CRISP code can provide good results for the total photonuclear absorption cross sections from approximately 50 MeV, where the quasi-deuteron absorption mechanism is dominant, up to 3.5 GeV, where the so-called photon-hadronization mechanism is dominant. It leads to a shadowing effect in the cross section [10]. One important feature in the simulation of the intranuclear cascade is the Pauli blocking mechanism, which avoids violation of the Pauli principle. In CRISP, a strict verification of this principle is performed at each step of the cascade, resulting in a more realistic simulation of the process. The advantages of such an approach have been further discussed elsewhere (see [3] and references therein).

In the evaporation/fission competition that follows intranuclear cascade, Weisskopf's model is adopted for calculating the branching ratios of the evaporating channels, which includes evaporation of neutrons, protons, and alpha-particles [6, 8, 9]. The Bohr-Wheeler model is adopted for the fission process. The code has provided photofission cross sections in full compliance to experimental data [3]. The CRISP code has already been used for evaluating mass distributions of fragments for fission induced by photons at intermediate energies [11], and to calculate spallation yields and neutron multiplicities for reactions induced by high energy protons [12], giving results in good agreement with experimental data. In addition, the code has already been used in studies of the ADS (Accelerator Driving System) nuclear-reactors [12–15].

III. DESCRIPTION OF MODEL AND CALCULATION

Theoretically, the fission process has been successfully described by the Multimodal - Random Neck Rupture Model (MM-NRM) [16–18], which takes into account the collective effects of nuclear deformation during fission through a liquid-drop model. Furthermore, it includes single-particle effects through microscopic shell-model corrections. The microscopic corrections create valleys in the space of elongation and mass number, each valley corresponding to one different fission mode [18].

The yield of fragments, characterized by A (the fragment mass number) and Z (the atomic number), is determined for each mode by a gaussian distribution. In the following we consider that the fission can take place through three modes: a symmetric mode and two asymmetric modes. The total yield is obtained by the sum of the three gaussian functions, as [19]:

$$\begin{aligned} Y_A &= \frac{1}{\sqrt{2\pi}}\left[\frac{K_{1AS}}{\sigma_{1AS}}\exp\left(-\frac{(A-\bar{A}_S-D_{1AS})^2}{2\sigma_{1AS}^2}\right)+\frac{K'_{1AS}}{\sigma'_{1AS}}\exp\left(-\frac{(A-\bar{A}_S+D_{1AS})^2}{2\sigma_{1AS}'^2}\right)+\right. \\ &\left.\frac{K_{2AS}}{\sigma_{2AS}}\exp\left(-\frac{(A-\bar{A}_S-D_{2AS})^2}{2\sigma_{2AS}^2}\right)+\frac{K'_{2AS}}{\sigma'_{2AS}}\exp\left(-\frac{(A-\bar{A}_S+D_{2AS})^2}{2\sigma_{2AS}'^2}\right)+\frac{K_S}{\sigma_S}\exp\left(-\frac{(A-\bar{A}_S)^2}{2\sigma_S^2}\right)\right], \end{aligned} \quad (1)$$

where $\bar{A}_S$ is the mean mass number determining the center of Gaussian functions; and K_i, σ_i, and D_i are the contribution, dispersion and position parameters of the i^{th} Gaussian functions. The indexes AS, S designate the asymmetric and symmetric components.

The fragment charge distribution can be estimated by using the approximation with Gaussian functions in the form [20, 21]:

$$Y_{A,Z} = \frac{Y_A}{\Gamma_z\pi^{1/2}}\exp\left(-\frac{(Z-Z_p)^2}{\Gamma_z^2}\right), \quad (2)$$

where $Y_{A,Z}$ is the independent yield of the nuclide (Z, A). The values Y_A (the total chain yield for given mass number A), Z_p (the most probable charge for Z distribution isobars with mass number A) and Γ_z (the width parameter). The values Z_p and Γ_z can be represented as slowly varying linear functions of the mass numbers of fission fragments:

$$Z_p = \mu_1 + \mu_2 A, \quad (3)$$
$$\Gamma_z = \gamma_1 + \gamma_2 A, \quad (4)$$

where μ_1, μ_2, γ_1 and γ_2 are adjustable parameters.

The yield, the position, and the width parameters for each mode in Eq. (1) and μ_1, μ_2, γ_1, and γ_2 in Eqs. (4) and (4) are usually considered free parameters for fitting procedure. This method has been used for describing spontaneous fission [22], low-energy induced fission [23–25], fission induced by thermal-neutrons [26–28] and 12 MeV protons [29], and even for fission induced by intermediate energy probes such as 190 MeV protons [21], neutrons at energies up to 200 MeV [30], and also by heavy-ions [31, 32].

Since the CRISP code simulates the entire process up to the point of fission, the fissioning nucleus of all events is known. Hence $\bar{A}_S$ is not taken as a free parameter, but as a distribution instead. Therefore, at every point of decision on the fission channel the appropriate value for $\bar{A}_S$ is used considering the nucleus which is undergoing fission.

Whenever the fission channel is chosen, the masses and atomic numbers of the heavy fragments produced, A_H and Z_H, respectively, are sorted according to equation (**??**). The light fragments are obtained according to $A_L = A_f - A_H$ and $Z_L = Z_f - Z_H$, where A_f and Z_f are the mass and atomic number of the fissioning nucleus, respectively.

As a final step, all fragments obtained in the above fashion evaporate according to the model of evaporation/fission competition already mentioned. The energy of each fragment is determined using

$$E_i = \frac{A_i}{A_f} E_{frag}, \tag{5}$$

where E_i and A_i are the excitation energy and the mass number of the fragment i, respectively. E_{frag} is the total excitation energy of the fragments, which is assumed to be equal to the excitation energy of the fissioning system.

IV. RESULTS AND DISCUSSION

In the induced fission of actinide nuclei, the target nucleus is initially excited by an incident beam. The nucleus may then reduce its excitation energy by emitted pre-scission neutrons and light charge particles. Eventually, the fission channel becomes more favorable, and scission occurs. The nascent fragments are accelerated by their mutual Coulomb repulsion and may themselves emit post-scission neutrons and γ-rays [33].

One way to obtain informations about the "hot" nuclear system and its decay channels is the study of the charge and mass characteristics of the fission products. In the off-line experiment usually it is detected fragments that represent the final products of the fission process after nucleons and gamma-rays emission from the fissioning nucleus and the primary fragments and the fragment β-decays. It is interesting also to compare the charge and mass yield distributions with those calculated by a CRISP intranuclear cascade-evaporation code for photonuclear reactions.

A. Charge Distribution

It is assumed that the charge distribution is well described by a gaussian function (2) and is characterized by parameters such as the most probable charge (Z_p) for the isobaric chains A and the width parameter (Γ_z). Experimental values of the most probable charge are removed from the line of β-stability by several charge units. With increasing of excitation energy and the atomic number of the fissioning nucleus, Z_p of isobaric chains becomes closer to the values Z for the stable nuclei. Another parameter that determines the charge distribution of the fragments, is the dispersion of the distribution, or the width parameter (Γ_z). Usually this parameter is averaged over the entire spectrum of the fragment mass numbers. With increasing excitation energy Γ_z values rises and charge distribution becomes broader. The parameters of the charge distribution determine the total isobaric yield of the mass, corresponding to different isobaric chains. In the experiment of present paper the width parameter Γ_z was assumed to be constant, irrespectively of A, and Z_p to be a linear function of A (3).

The full width at half maximum of the charge distribution ($FWHM$) in charge unit instead of Γ_z and the parameters μ_1 and μ_2 are shown in a Table 1 for Bremsstrahlung end-point energies 50 and 3500 MeV, together with calculated values by CRISP code (3), (4).

Table 1. Parameters of the charge distributions.

Parameter	^{238}U		^{232}Th	
	$E_{max} = 50$ MeV	$E_{max} = 3500$ MeV	$E_{max} = 50$ MeV	$E_{max} = 3500$ MeV
$(\mu_1)_{exp}$	5.70±0.60	5.32±0.62	3.89±0.67	4.14±0.70
$(\mu_2)_{exp}$	0.356±0.005	0.362±0.005	0.371±0.005	0.356±0.005
$(\mu_1)_{cal}$	4.1	4.1	5.0	5.0
$(\mu_2)_{cal}$	0.38	0.38	0.37	0.37
$(\gamma_1)_{cal}$	0.92	0.92	0.59	0.59
$(\gamma_2)_{cal}$	0.003	0.003	0.005	0.005
$FWHM$	1.03±0.12	1.09±0.13	1.13±0.14	1.14±0.15

From the data of $FWHM$ in Table 1, it is clear that as the excitation energy increases, the charge distribution becomes wider. Furthermore, the absolute value of the parameter changes slightly, according to the variation of the energy, within the accuracy considered. The deviation of experimental widths from the values calculated for the targets ^{238}U and ^{232}Th at two end-point energies is plotted in Figure 1 (a, b). The values for χ^2 are as follows: in the case of ^{238}U: $\chi^2 = 0.63$, $E_{max} = 50$ MeV and $\chi^2 = 0.43$ for $E_{max} = 3500$ MeV; in the case of ^{232}Th: $\chi^2 = 0.45$ for $E_{max} = 50$ MeV; $\chi^2 = 0.71$ at $E_{max} = 3500$ MeV.

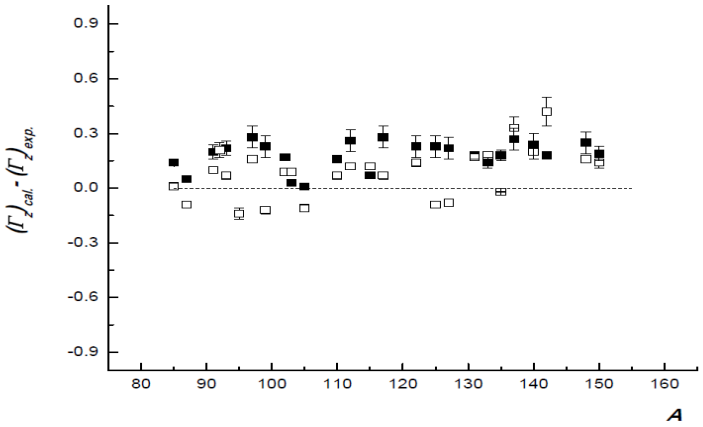

a)

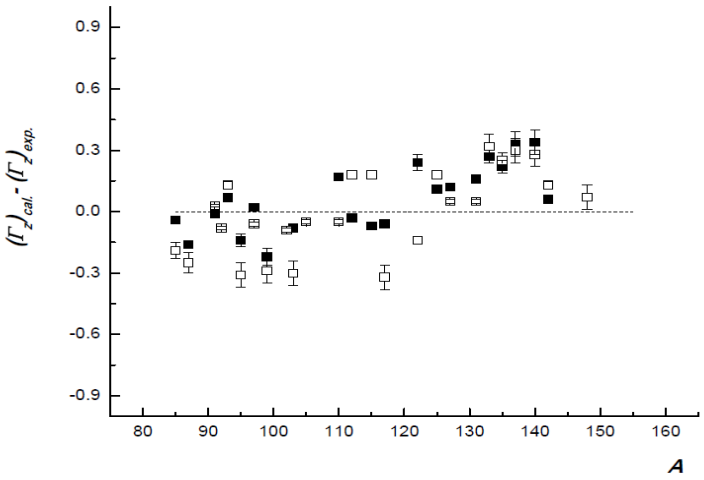

b)

FIG. 1: The deviation of experimental width of charge distribution from calculated by CRISP code for ^{238}U (a) and ^{232}Th (b) targets; □ – $E_{max} = 50$ MeV, ■ – $E_{max} = 3500$ MeV.

Figure 2 shows both the experimental values of the most probable charge Z_p and the values, calculated by the CRISP model for ^{238}U (a, b) and ^{232}Th (c, d) at two incident energies. In general, the experimental values of Z_p fit well to that obtained by model calculations (^{238}U: $\chi^2 = 0.022$, $E_{max} = 50$ MeV and $\chi^2 = 0.014$ for $E_{max} = 3500$ MeV; ^{232}Th: $\chi^2 = 0.011$ for $E_{max} = 50$ MeV; $\chi^2 = 0.007$ at $E_{max} = 3500$ MeV).

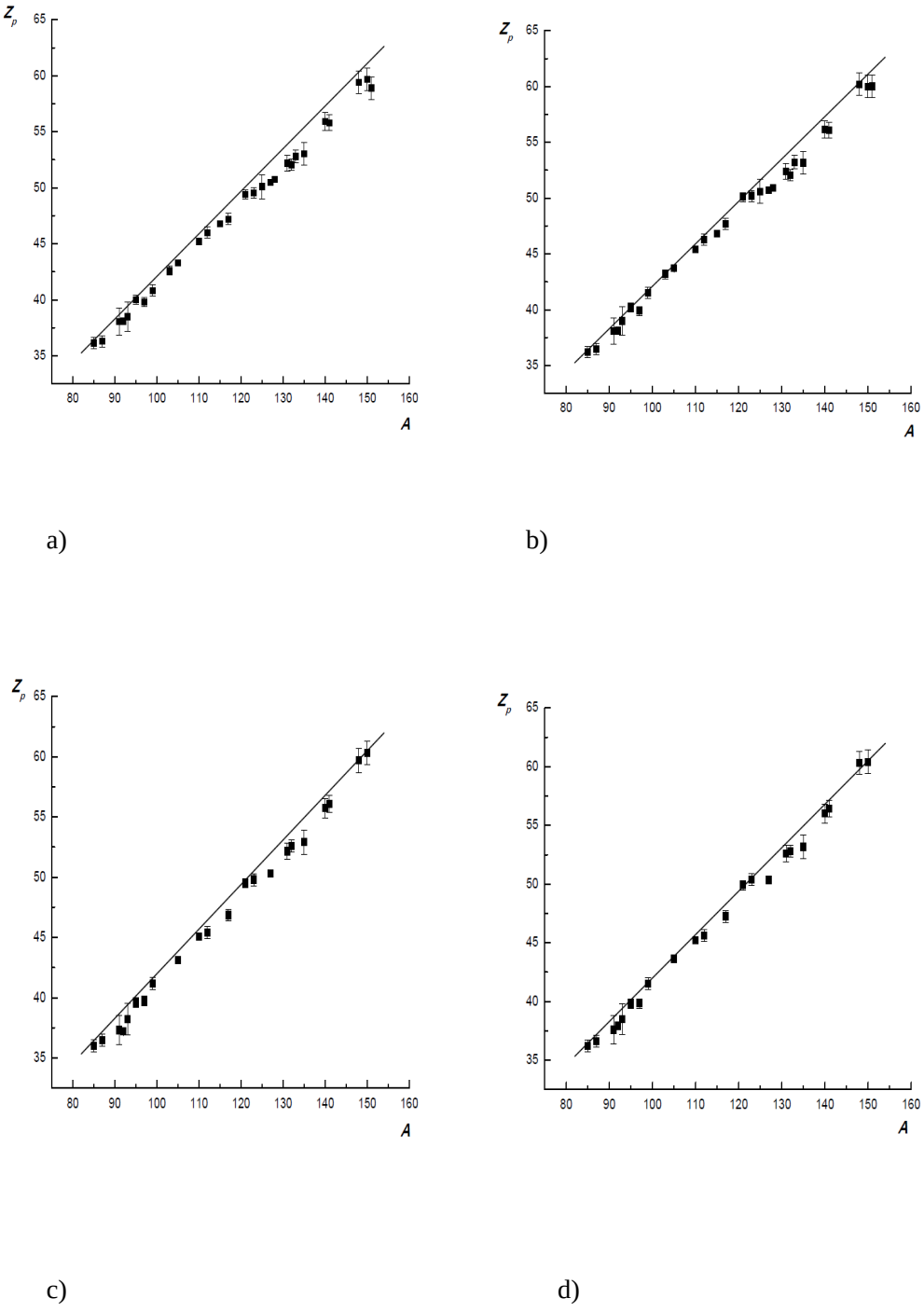

FIG. 2: The most probable charge Z_p for ^{238}U (a, b) and ^{232}Th (c, d) targets at Bremsstranhlung end-point energies 50 (a, c) and 3500 MeV (b, d), respectively: the calculations by CRISP (thick black solid line), experimental data (■).

However, as can be seen from the Figure 2, the experimental charges shifts to the proton-deficient side relative to the model predictions. Significant deviation at low energies is observed for symmetric fission near $A = 125 - 130$. This may be a manifestation of the fragment shell effect ($Z_p \sim 50$), which is smeared with energy [34].

Agreement with calculation values becomes better, especially, for the nucleus ^{232}Th and mainly in the range of symmetric fission, where the contributions of high-energy neutron-deficient fissioning nuclei is larger.

The agreement between calculation and experiment improves for higher excitation energies. A significant shift of the Z_p to higher values for the heavy mass numbers is mentioned. Increasing the value of Z_p is due to the excitation energy of the fissioning nucleus, which is distributed proportional to the mass of the fragments. As a consequence, on average, more neutrons evaporates from the heavy fragments, than from light ones. That is why at intermediate energies, experimental Z_p shifts to values that are near to calculated (see criterion χ^2).

Analysis of parameter values shows that in general, the CRISP model fairly well describes the charge distribution for the fission fragments for ^{232}Th, and for ^{238}U. It can be assumed that the model takes into account the main properties of fissile systems and provide a universal way to predict the characteristics of the fragment charge distribution.

B. Mass Distribution

Mass distributions of the fissioning nuclei are very different in shape for different mass ranges. The excitation energy of the fissioning system plays an important role in the dynamics of the fission process. The origin of the asymmetric fission is associated with the shell structure of the fissioning nucleus and nuclear fragments [35]. Whereas symmetric fission is consistent with the classical liquid-drop picture of the fissioning nucleus [36].

The application of the hypothesis of the multicomponent fission allowed to extract different components on the base of decomposition of the mass yield curve (Eq. (1)). According to this model [18] the mass-yield curve can be decomposed into distinct fission components: one symmetric Superlong and two asymmetric Standard I, Standard II. Superlong mode fragments are strongly elongated with masses around $A_f/2$. Standard I mode is characterized by influence spherical neutron shell $N_H \sim 82$ and proton shell $Z_H \sim 50$ in the heavy fragments with masses $M_H \sim 132 - 134$. Standard II mode is characterized by influence the deformed neutron shell closure $N = 86 - 88$ and proton shell $Z_H \sim 52$ in the heavy fragments with masses $M_H \sim 138 - 140$.

By using the calculated values of Y_A that correspond to the total yield of fission fragments for a specific mass number (2) made it possible to construct the mass yield at two energies of the Bremsstrahlung spectrum. Integrating over the Gaussian and multiplying with a factor 0.5, because of the two fission fragments in each fission event, gives an estimate for the total fission yield Y_{tot}. The values for the total fission yields determined in this way together with calculated by CRISP code are given in Table 2. In Table 2 the following values are also given: the position of the two humps, A_L and A_H, at the peaks of asymmetric fission; the mean mass of the mass distribution ($\bar{A}_S$); mean mass of the fissioning nucleus ($(A_f)_{cal}$) after evaporation of pre-scission neutrons from compound nucleus; mean mass of the fissioning nucleus ($(A_{ff})_{cal}$) after evaporation of post-scission neutrons from fragments; experimental mean mass of the fissioning nucleus ($(A_f)_{exp}$), corresponding to neutrons emission before and after fission; the values of the peak-to-valley ratios (P/V). The total fission mass-yield distributions at $E_{max} = 50$, 3500 are shown in Figure 3 (a, b) and Figure 4 (a, b), respectively, as a function of the product mass number (A) for ^{238}U and ^{232}Th targets.

Table 2. Parameters of the mass distributions.

Parameter	^{238}U		^{232}Th	
	E_{max} = 50 MeV	E_{max} = 3500 MeV	E_{max} = 50 MeV	E_{max} = 3500 MeV
$(Y_{tot})_{exp}$, $mb/eq.q$	131.6±19.5	250.1±37.5	40.2±6.0	137.5±20.6
$(Y_{tot})_{cal}$, $mb/eq.q$	149	268.8	39.6	129.6
$(P/V)_{exp}$	11.41±1.71	2.16±0.40	7.93±1.59	0.84±0.17
$(P/V)_{cal}$	10.63	6.45	4.80	1.45
$(A_L)_{exp}$	98.0±1.9	97.0±1.9	91.5±1.8	94.0±1.8
$(A_L)_{cal}$	98.0	95.0	94.0	95.5
$(A_H)_{exp}$	137.0±2.7	137.0±2.7	137.5±2.7	134.0±2.6
$(A_H)_{cal}$	136.0	133.0	134.0	124.5
$(\bar{A}_S)_{exp}$	117.5±0.2	117.0±0.2	114.5±0.3	114.0±0.3
$(\bar{A}_S)_{cal}$	117.0	114.0	114.0	110.0
$(A_f)_{exp}$	235.0	234.0	229.0	228.0
$(A_{ff})_{cal}$	234.0	228.0	228.0	220.0
$(A_f)_{cal}$	237.55	235.95	230.61	227.70

The results by CRISP code calculations allowed to do an overview of the distributions for ^{238}U and ^{232}Th. Qualitatively, the agreement between the calculation and the experimental data is fairly good at both end-point energies. Especially, it is clear shown for low energies, where the calculations reproduce the experimental features quite well. This fact shows that the model correctly takes into account the influence of shell effects at low energy fission, associated with asymmetric fission mode: the strong spherical neutron shell at $N = 82$ and the deformed neutron shell at $N = 86 - 88$ become dominant and lead to asymmetric fission. There is a small deviation between experimental and calculated values in height and position of two peaks at $E_{max} = 50$ for ^{232}Th target. It can be explained by the different contribution of symmetric fission mode for calculated yield and experimental one. The calculations takes into account more nucleons evaporation before actual fission for ^{232}Th, therefore the probability of symmetric fission for calculated yield is higher than for uranium target.

The systematization of cross-sections for symmetric and asymmetric fission in a wide range of nuclei (from $Z = 80$ to $Z = 105$) at the energy up to hundreds MeV, carried out in [37, 38]. It was considered that it is possible to use an empirical expression for estimating the probability of the different fission modes. Such approach was based on the observation that the symmetric component increases with excitation energy. In order to characterize this factor quantitatively, the authors introduced a critical value of the fissility parameter, in the form:

$$(Z^2/A)_{cr.} = 35.5 + 0.4(Z_f - 90). \quad (6)$$

According to [37, 38], for the nuclei with Z^2/A values greater than the critical value, the symmetric fission mode was dominant, but at smaller values of the fissility parameter, the main fission channel leads to asymmetric fragments. Such approach is based on the observation that the symmetric component increases with excitation energy. For ^{238}U nucleus parameter $(Z^2/A)_{cr.}$ is 36.3, and for the ^{232}Th is 35.5. Thus, at low energy (with an average of no more than three evaporated neutrons) for ^{238}U it is natural to expect predominantly asymmetric fission.

At intermediate energies the deviation between the calculated and the experimental values becomes larger for all observed parameters, excluding the total fission yields. The reason of it could be explained from the character of Bremsstrahlung. As the later has a continuous spectra, the measurements at high energy include also low-energy photons. From the calculated mass distribution it can be concluded that the model underestimates the low-energy part of Bremsstrahlung. As the energy increases, the mean mass number of distributions calculated after the evaporation of post-scission neutrons $(A_f)_{cal}$ are shifted to lower masses, compared to the experimental ones. It means that the yields of symmetric fission fragments grow faster, because of considerable amount of high-energy photons.

The observation that the symmetric component increases with excitation energy can be explained by several factors. First of all, the impact of shell effects becomes less pronounced as the energy increases [39]. On the another hand, a higher excitation energy is coupled to an increment of the neutron evaporation. In the case of interactions with intermediate- and high-energy particles, the fission process is considered at a slow reaction stage after the completion of the internuclear cascade and the formation of a set neutron-deficient fissioning nuclei with higher fissility parameter. Neutron evaporation is a process that competes with the fission process (proton emission is suppressed). These processes proceed sequentially in several steps, depending on the excitation energy. At each step, the residual nucleus may undergo fission or/and emit a neutron [21, 30, 37, 38].

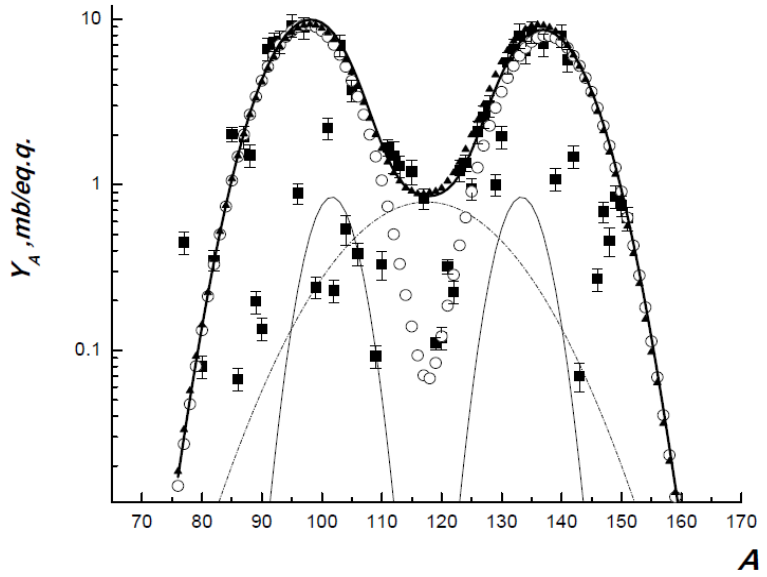

a)

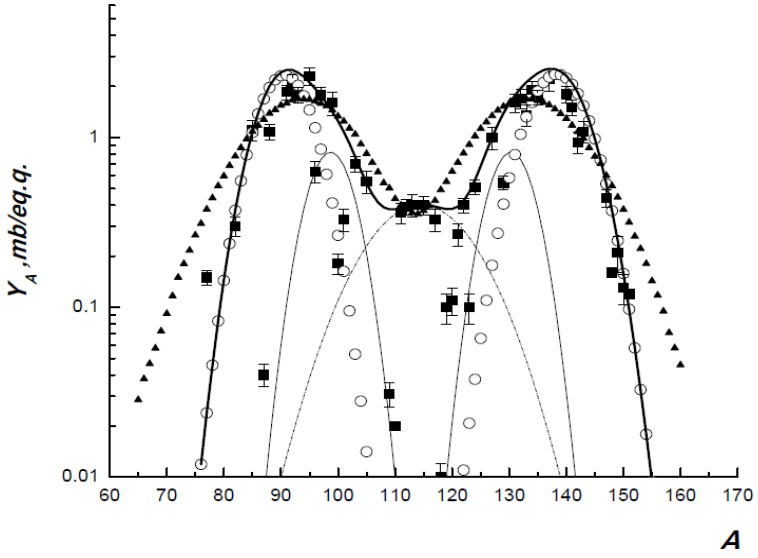

b)

FIG. 3: Components of mass yield at E_{max} = 50 MeV for ^{238}U (a) and ^{232}Th (b) targets: Superlong mode(dash-dot line), Standard I mode (thin line), Standart II (○), total experimental yield $(Y_{tot})_{exp}$ (thick line), total calculated yield $(Y_{tot})_{cal}$ (▲), experimental points (■).

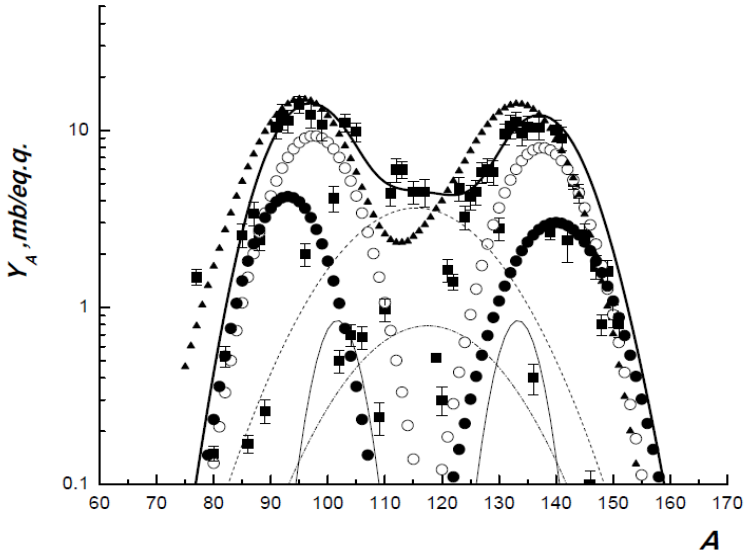

a)

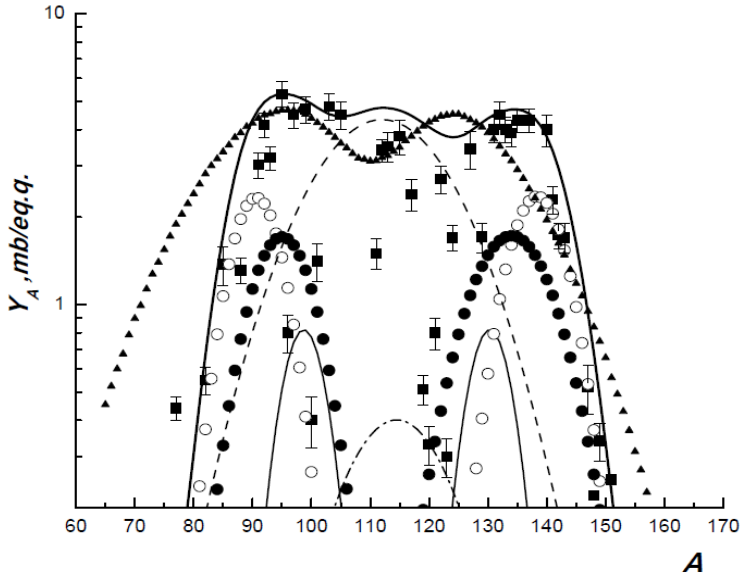

b)

FIG. 4: Components of mass yield at $E_{max} = 3500$ MeV. Symbols, corresponding to the low energy fission yield are the same as Fig. 3; the high energy components are: asymmetric mode(●), symmetric mode (dot line),total experimental yield $(Y_{tot})_{exp}$ (thick line), total calculated yield $(Y_{tot})_{cal}$ (▲), experimental points (■).

From the mean mass of the calculated mass distributions it can be concluded that ten and twelve mass units are emitted in average, from ^{238}U and ^{232}Th targets, respectively. It is much greater than the corresponding experimental values. Due to 6 one can suggest that the contribution of sequential multichance [30, 40] fission of neutron-deficient fissioning nuclei in case of ^{232}Th is larger.

From the Table 2, we can see that the mean masses of the fissioning nuclei $(A_f)_{cal}$ after evaporation of pre-scission neutrons are different from the target nuclei, due to the emission of particles during the intranuclear cascade and the pre-equilibrium steps before fission as well.

The mass distributions for the fissioning nuclei ^{238}U and ^{232}Th for photon-induced fission calculated at 50 and 3500 MeV are shown in Figure 5 (a, b, c, d), respectively. More realistic calculations were obtained for ^{232}Th target. It is almost the same in the case of intermediate-energy photons.

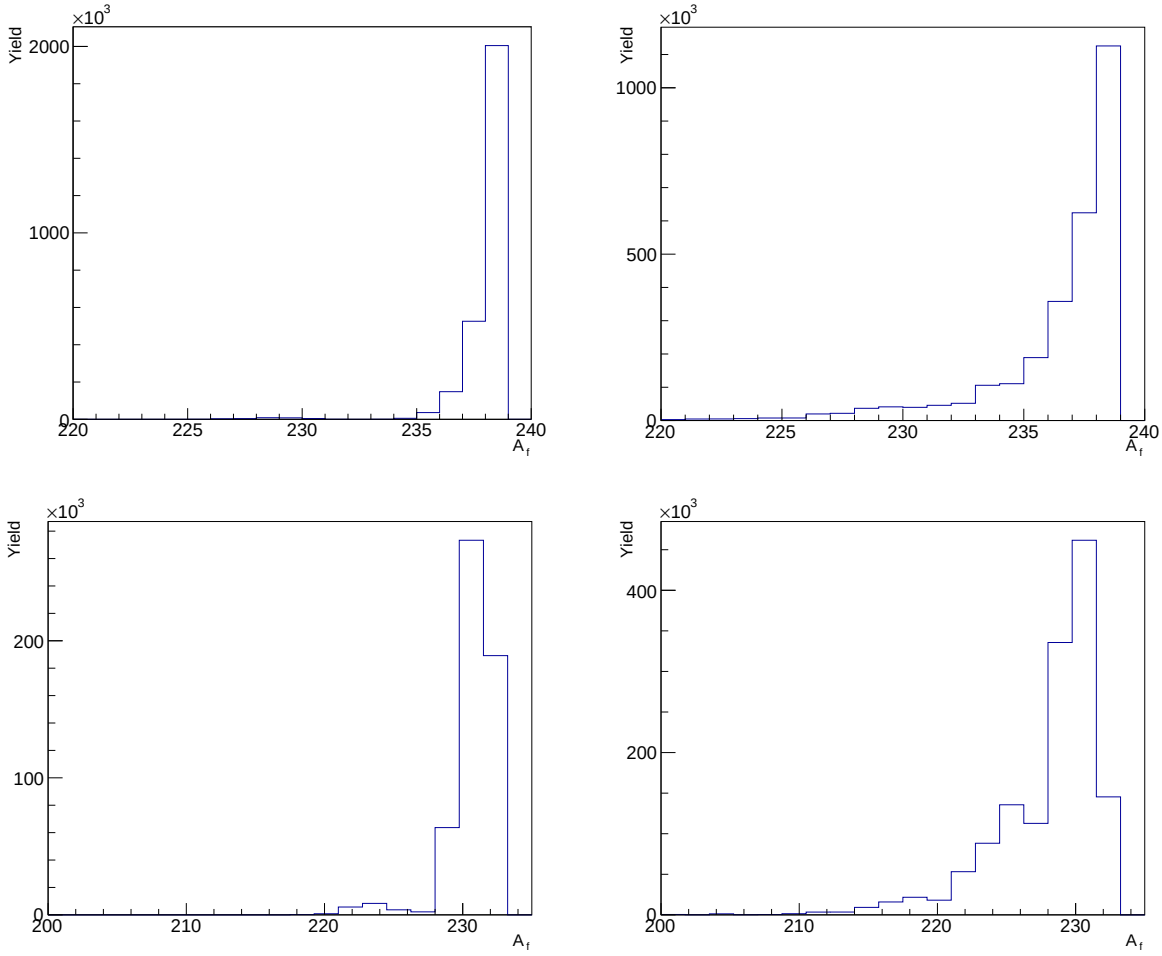

FIG. 5: Mass distributions of the fissioning nuclei for ^{238}U (a, b) and ^{232}Th (c, d) targets at bremsstrahlung end-point energies 50 (a, c) and 3500 MeV (b, d).

Calculation by CRISP code made it possible to estimate the fissility for photon-induced fission and compare it with experimental. According to the well-known concept, the fissility is determined as the ratio of the fission yield and the yield of total photon absorption in a nucleus (D=Y_{tot}/Y_{abs}). The dependence of fissility for ^{238}U and ^{232}Th target of the present together with data for proton-induced fission of ^{241}Am, ^{238}U and ^{237}Np nuclei from [41, 42] on parameter Z^2/A of fissioning nucleus is shown on Fig. 6 together with calculations data by CRISP code. One can see that the fission probabilities are about the same, independently of the tool used to excite the nuclear matter and the fissility of heavier element is getting larger. The calculated data of fissility for thorium target fitted well enough to the experimental values at both energies within the experimental uncertainties and increased up to a value 0.45 upon going over from low to intermediate energies. There is another situation in case of uranium target: the calculated values of the fissility at both energies overestimate the experimental ones, especially it is clear shown at low energy of

photons. Such discrepancy may originated because the model doesn't take into account all possible channels of decay of the excited nucleus being considered.

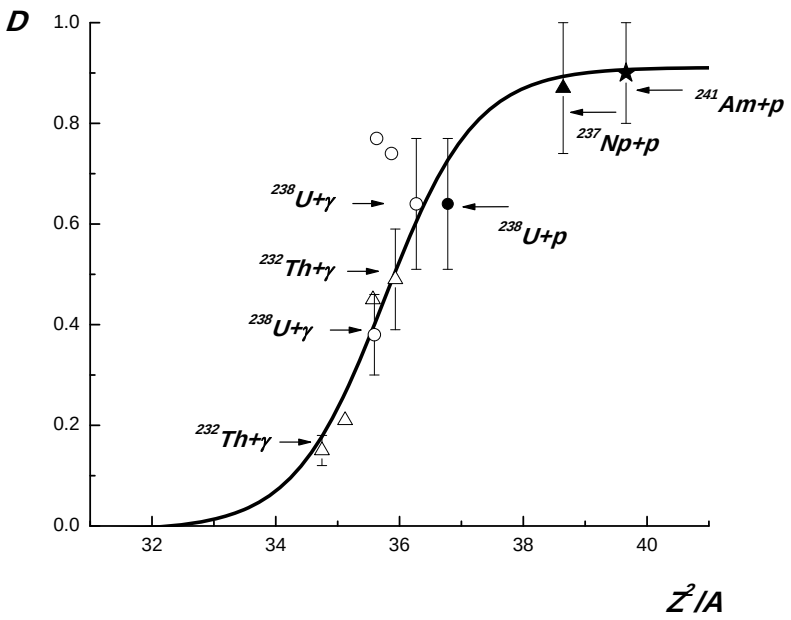

FIG. 6: Z^2/A dependence of fissility D. Presented symbols for experimental data are: p+^{237}Np (▲) [41, 42] , p+^{238}U (•) [41, 42], p+^{241}Am (⋆) [41, 42], γ+^{238}U (○)–present work, γ+^{232}Th (△)–present work. Calculations by CRISP are symbols without errors: γ+^{238}U (○), γ+^{232}Th (△). The solid line is to guide the eye the experimental points.

V. CONCLUSION

The modified CRISP model calculations, which takes into account different channel of fission, was used to reproduce different aspects of photon-induced fission on actinides. Those calculations allow a direct evaluation of the spectrum of fissioning nuclei. The comparison with the calculated data was shown, evincing that the calculations describe correctly the main characteristics of charge distribution, such as the most probable charge for a given fission product mass chain and the width parameter. The mass yield of photofission fragments has been analyzed via multimodal fission approach. The results presented in this paper shows a fair agreement between calculation and experiment. The results of the calculations made it possible to determine the fissilities of the fissioning nuclei and compare it with those from experiments.

It was found that CRISP simulations better reproduce data for low-energy photon-induced fission neutron-deficient fissioning systems.

Acknowledgment

G. Karapetyan is grateful to Fundação de Amparo à Pesquisa do Estado de São Paulo (FAPESP) 2011/00314-0. and to International Centre for Theoretical Physics (ICTP) under the Associate Grant Scheme.

[1] N. A. Demekhina and G. S. Karapetyan, Phys. At. Nucl. **71**, 27 (2008).
[2] N. A. Demekhina and G. S. Karapetyan, Phys. At. Nucl. **73**, 24 (2010).
[3] A. Deppman, S. B. Duarte, G. Silva, *et al.*, J. Phys. G: Nucl. Part. Phys. **30** 1991 (2004).
[4] T. Kodama, S. B. Duarte, K. C. Chung, *et al.*, Phys. Rev. Lett. **49**, 536 (1982).
[5] M. Goncalves, S. dePina, D. A. Lima, *et al.*, Phys. Lett. B **406**, 1 (1997).

[6] A. Deppman, O. A. P. Tavares, S. B. Duarte, *et al.*, Phys. Rev. Lett. **87**, 1 (2001).
[7] S. de Pina, *et al.*, Phys. Lett. B **434**, 1 (1998).
[8] A. Deppman, O. A. P. Tavares, S. B. Duarte, *et al.*, Comp. Phys. Comm. **145**, 385 (2002).
[9] A. Deppman, O. A. P. Tavares, S. B. Duarte, *et al.*, Phys. Rev. C **66**, 067601 (2002).
[10] A. Deppman, G. Silva, S. Anefalos, *et al.*, Phys. Rev. C **73**, 1 (2006).
[11] E. Andrade-II, E. Freitas, O. A. P. Tavares, *et al.*, *Proc. Conf. on XXXI Worshop on Nuclear Physics in Brazil* **1139**, 64 (2009).
[12] S. A. Pereira, *et al.*, Nuc. Sci. and Eng. **159**, 102 (2008).
[13] S. Anefalos, A. Deppman, G. Silva, *et al.*, 2005 Braz. J. Phys. **35**, 912 (2005).
[14] S. Anefalos, A. Deppman, J. D. T. Arruda-Neto, *et al.*, *Proceedings of Int. Conf. on Nuclear Data for Science and Technology* **769**, 1299 (2004).
[15] S. T. Mongelli, J. R. Maiorino, S. Anefalos, *et al.*, Braz. J. Phys. **35**, 894 (2005).
[16] V. V. Pashkevich, Nucl. Phys. A **169**, 275 (1971).
[17] B. D. Wilkins, E. P. Steinberg, and R. R. Chasman, Phys. Rev. C **14**, 1832 (1976).
[18] U. Brosa, S. Grossman, and A. Muller, Z. Naturforschung **41a**, 1341 (1986).
[19] W. Younes, J. A. Becker, L. A. Bernstein, *et al.*, *CP610, Proceedings of Int. Nucl. Conf., INPC (2001).*
[20] H. Kudo, M. Maruyama, M. Tanikawa, *et al.*, Phys. Rev. C **57**, 178 (1998).
[21] M. C. Duijvestijn, A. J. Koning, *et al.*, Phys. Rev. C **59**, 776 (1999).
[22] C. Wagemans, P. Schillebeeckx and A. Deruytter, Nucl. Phys. A **502**, 287 (1989).
[23] Th. Weber, *et al.*, Nucl. Phys. A **502**, 279 (1989).
[24] J. L. Sida, *et al.*, Nucl. Phys. A **502**, 233 (1989).
[25] C. Bockstiegel , S. Steinhauser, K.-H. Schimdt, *et al.*, Nucl. Phys. A **802**, 12 (2008).
[26] F. J. Hambsch, *et al.*, Nucl. Phys. A **709**, 85 (2002).
[27] F. J. Hambsch, *et al.*, Nucl. Phys. A **726**, 248 (2003).
[28] H. Weigmann, H. H. Knitter and F. J. Hambsch, Nucl. Phys. A **502**, 177 (1989).
[29] T. Ohtsuki, *et al.*, Phys. Rev. C **40**, 2144 (1989).
[30] V. M. Maslov, Nucl. Phys. A **717**, 3 (2003).
[31] M. G. Itkis, *et al.*, Z. Phys. A **320**, 433 (1985).
[32] I. V. Pokrovsky, *et al.*, Phys. Rev. C **62**, 1 (2000).
[33] M. Strecker, *et al.*, Phys. Rev. C **41**, 2172 (1990).
[34] M. Brack, *et al.*, Rev. Mod. Phys. **44**, 320 (1972).
[35] V. M. Strutinsky, Nucl. Phys. A **122**, 1 (1968).
[36] W. D. Myers and W. J. Swiatecki, Nucl. Phys. **81**, 1 (1966).
[37] C. Chung and J.Hogan, Phys. Rev. C **24**, 180 (1981).
[38] C. Chung and J.Hogan, Phys. Rev. C **25**, 899 (1982).
[39] V. A. Rubchenya, Phys. Rev. C **75**, 054601 (2007).
[40] P. David, J. Debrus, *et al.*, Nucl. Phys. A **197**, 16 (1972).
[41] G. S. Karapetyan, A. R. Balabekyan, N. A. Demekhina, and J. Adam, Phys. At. Nucl. **72**, 911 (2009).
[42] A. R. Balabekyan, G. S. Karapetyan, N. A. Demekhina, *et al.*, Phys. At. Nucl. **73**, 1814 (2010).